

# **Environmental Security Technology Certification Program (ESTCP)**

## **Final Wide Area Assessment Demonstration of LiDAR and Orthophotography at Borrego Maneuver Area**



### **Project No. ESTCP-200416 Phase II Innovative Multi-Sensor Airborne Wide Area Assessment of UXO Sites**

**December 3, 2007  
Version: 2.0**

<b>REPORT DOCUMENTATION PAGE</b>					<i>Form Approved</i> <i>OMB No. 0704-0188</i>	
The public reporting burden for this collection of information is estimated to average 1 hour per response, including the time for reviewing instructions, searching existing data sources, gathering and maintaining the data needed, and completing and reviewing the collection of information. Send comments regarding this burden estimate or any other aspect of this collection of information, including suggestions for reducing the burden, to the Department of Defense, Executive Services and Communications Directorate (0704-0188). Respondents should be aware that notwithstanding any other provision of law, no person shall be subject to any penalty for failing to comply with a collection of information if it does not display a currently valid OMB control number.						
<b>PLEASE DO NOT RETURN YOUR FORM TO THE ABOVE ORGANIZATION.</b>						
<b>1. REPORT DATE (DD-MM-YYYY)</b> 12-03-2007		<b>2. REPORT TYPE</b> Draft Final			<b>3. DATES COVERED (From - To)</b> May 2005 - December 2006	
<b>4. TITLE AND SUBTITLE</b> Draft Final Report Wide Area Assessment Demonstration of LiDAR and Orthophotography at Borrego Maneuver Area				<b>5a. CONTRACT NUMBER</b> W912HQ-05-C-0036		
				<b>5b. GRANT NUMBER</b>		
				<b>5c. PROGRAM ELEMENT NUMBER</b> MM-0416		
				<b>5d. PROJECT NUMBER</b>		
<b>6. AUTHOR(S)</b> Dr. Jack Foley				<b>5e. TASK NUMBER</b>		
				<b>5f. WORK UNIT NUMBER</b>		
<b>7. PERFORMING ORGANIZATION NAME(S) AND ADDRESS(ES)</b> Sky Research, Inc. 445 Dead Indian Memorial Dr. Ashland, OR 97520					<b>8. PERFORMING ORGANIZATION REPORT NUMBER</b>	
<b>9. SPONSORING/MONITORING AGENCY NAME(S) AND ADDRESS(ES)</b> Environmental Security Technology Certification Program Office 901 North Stuart Street, Suite 303 Arlington, VA 22203-1821					<b>10. SPONSOR/MONITOR'S ACRONYM(S)</b> ESTCP	
					<b>11. SPONSOR/MONITOR'S REPORT NUMBER(S)</b>	
<b>12. DISTRIBUTION/AVAILABILITY STATEMENT</b> Unlimited						
<b>13. SUPPLEMENTARY NOTES</b>						
<b>14. ABSTRACT</b> This report describes the data collection, methodology and analysis conducted by Sky Research for the LiDAR and digital orthophotography high airborne sensor technologies demonstrated at Borrego Maneuver Area (BMA) in California. LiDAR data are critical to the overall WAA process in several roles: creation of an accurate high-resolution bare earth digital elevation model (DEM) for ortho-correction of all other remote-sensing datasets; extraction of possible surface munitions related features and for base mapping layers for site visualization, planning and analysis. Orthophotography is valuable for direct detection and visualization of possible munitions related features; as input to multiple-sensor fusion algorithms for surface feature detection; and for site visualization and planning. Data processing and analysis of the collected data sets resulted in the detection of target areas and range infrastructure features at the site. The performance assessment results show that while most features can be detected in the datasets, erosion and wind can obscure features over time.						
<b>15. SUBJECT TERMS</b> Wide Area Assessment, orthophotography, LiDAR, remote sensing, Borrego Maneuver Area, Borrego Military Wash, munitions related features, digital elevation model						
<b>16. SECURITY CLASSIFICATION OF:</b> a. REPORT b. ABSTRACT c. THIS PAGE			<b>17. LIMITATION OF ABSTRACT</b>		<b>18. NUMBER OF PAGES</b> 49	
<b>19a. NAME OF RESPONSIBLE PERSON</b> Dr. John Foley					<b>19b. TELEPHONE NUMBER (Include area code)</b> 541.552.5141	

Reset

## Table of Contents

List of Figures .....	ii
List of Tables .....	ii
Acronyms .....	iii
1. Introduction .....	1
1.1 Background .....	1
1.2 Objectives of the Demonstration .....	2
1.3 Regulatory Drivers .....	2
1.4 Stakeholder/End User .....	2
2. Technology Description .....	5
2.1 Technology Development and Application .....	5
2.2 Previous Testing of the Technology .....	8
2.3 Factors Affecting Cost and Performance .....	8
2.4 Advantages and Limitations of the Technology .....	9
3. Demonstration Design .....	10
3.1 Performance Objectives .....	10
3.2 Test Site Selection .....	11
3.3 Test Site History/Characteristics .....	11
3.4 Pre-Demonstration Testing and Analysis .....	12
3.5 Testing and Evaluation Plan .....	15
3.6. Data Processing .....	19
3.7. Data Analysis .....	23
4. Performance Assessment .....	27
4.1 Spatial Accuracy .....	27
4.2 Data Analysis Results .....	28
4.3 Performance Criteria .....	34
4.4 Performance Confirmation Methods .....	35
4.5 Performance Assessment Summary .....	40
5. Cost Assessment .....	42
5.1 Cost Analysis .....	42
5.2 Cost Reporting .....	43
6. Implementation Issues .....	44
7. Points of Contact .....	45
Appendix A: Optech ALTM 3100 Specifications .....	A-1
Appendix B: ALTM 4K X 4K Digital Camera Specifications .....	B-1
Appendix C: Sky Research LiDAR Sensor Calibration Plot .....	C-1

## List of Figures

Figure 1 - C208 fixed-wing platform houses the orthophotography and LiDAR sensors for concurrent data collection. ....	3
Figure 2 - The WAA demonstration was conducted in sub-areas E-1 and E-2 of the Borrego Military Wash of the former BMA. ....	13
Figure 3 - Collection area and study area boundaries for LiDAR and orthophotography data collection at BMA. ....	14
Figure 4 - Example of a calibration site crater with a diameter of 0.75 m and depth of 0.4 m. ..	16
Figure 5 – Crater calibration area at the Sky Research facility in Ashland, Oregon. ....	16
Figure 6 - Location of base stations for high airborne remote sensing data collection at BMA. .	17
Figure 7 - Screenshot of ISAT aerotriangulation results window. ....	22
Figure 8 - Screenshot of OrthoPro seam lines (pink), tiles (blue), and photos (green). ....	22
Figure 9 - Munitions related features detected at BMA utilizing high airborne orthophotography and LiDAR datasets. ....	29
Figure 10 - Extracted circular aiming point target features for BT64 shown on color orthophoto. ....	30
Figure 11 - Extracted railroad strafing target shown on the color orthophoto image. ....	31
Figure 12 - Large-scale views of the rake station range infrastructure features. ....	33
Figure 13 - Small depression detected in data and identified as a feature of interest. ....	34
Figure 14 - Outline of target circle as photographed during visual reconnaissance survey. ....	37
Figure 15 - 100 lb bomb scrap as photographed in target circle during visual reconnaissance survey. ....	37
Figure 16 - Partially buried target in small depression detected during data analysis. ....	38
Figure 17 - Munitions scrap found in small depression area. ....	38
Figure 18 - Concrete rake station. ....	39
Figure 19 - 20 mm located in concrete of rake station. ....	39

## List of Tables

Table 1	LiDAR Specifications .....	4
Table 2	Orthophotography Specifications .....	6
Table 3	Primary Performance Objectives .....	10
Table 4	Secondary Performance Objectives .....	11
Table 5	Acquisition Parameters for BMA LiDAR Survey .....	18
Table 6	LiDAR and Orthophotography Data Accuracy Results .....	27
Table 7	Performance Criteria .....	34
Table 8	Performance Confirmation Methods and Results .....	35
Table 9	Cost Tracking.....	42
Table 10	Points of Contact.....	45

## Acronyms

3D	Three dimensional
AGL	Above Ground Level
ASR	Archive Search Report
BMA	Borrego Maneuver Area
BT64	Bomb Target 64
C208	Cessna 208
CCD	Charged Coupled Device
CERCLA	Comprehensive Environmental, Response, Compensation, and Liability Act
cm	centimeter(s)
CSM	Conceptual Site Model
DEM	Digital Elevation Model
DoD	Department of Defense
DSB	Defense Science Board
DTM	Digital Terrain Model
ESRI	Environmental Systems Research Institute
ESTCP	Environmental Security Technology Certification Program
FLBGR	Former Lowry Bombing and Gunnery Range
FUDS	Formerly Used Defense Sites
GIS	Geographic Information Systems
GB	gigabyte
GPS	Global Positioning System
HE	High Explosive
HVAR	High Velocity Air Rocket
Hz	Hertz
ID	identification
IDL	Interactive Data Language
IMU	Inertial Measurement Unit
ISAT	ImageStation Auto Triangulation
km	kilometer(s)
LiDAR	Light Detection and Ranging
m	meter(s)
MMRP	Military Munitions Response Program
MRF	Munitions Related Feature
NAD83	1983 North American Datum
PDOP	Position Dilution of Precision
POS	Position and Orientation
RGB	Red-Green-Blue
RI/FS	Remedial Investigation and Feasibility Study
RMSE	Root Mean Square Error
RTK GPS	Real-time Kinematic GPS
RTS	Robotic Total Station

SBET	Smooth Best Estimate Trajectory
TNT	Trinitrotoluene
USACE	United States Army Corps of Engineers
UTM	Universal Transverse Mercator
UXO	Unexploded Ordnance
WAA	Wide Area Assessment
WAA-PP	Wide Area Assessment Pilot Program

# **1. Introduction**

## **1.1 Background**

Unexploded ordnance (UXO) contamination is a high-priority problem for the Department of Defense (DoD). Recent DoD estimates of UXO contamination across approximately 1,400 DoD sites and formerly used defense sites (FUDS) indicate that 10 million acres are suspected of containing UXO. Because many sites are large in size (greater than 10,000 acres), the cost of investigation and remediation of these sites could exceed billions of dollars. However, on many of these sites only a small percentage of the site may in fact contain UXO contamination. Therefore, determining applicable technologies to define the contaminated areas requiring further investigation and munitions response actions could provide significant cost savings. Therefore, the Defense Science Board (DSB) has recommended further investigation and use of Wide Area Assessment (WAA) technologies to address the potential these technologies offer in terms of determining the actual extent of UXO contamination on active DoD sites and FUDS.

In response to the DSB Task Force report and recent Congressional interest, the Environmental Security Technology Certification Program (ESTCP) designed a Wide Area Assessment Pilot Program (WAA-PP) that consists of demonstrations at multiple sites to validate the application of a number of recently developed and validated technologies as a comprehensive approach to WAA. These demonstrations of WAA technologies include deployment of high airborne sensors, helicopter-borne magnetometry arrays and ground surveys.

This report describes the data collection, methodology and analysis conducted by Sky Research for Light Detection and Ranging (LiDAR) and orthophotography high airborne sensor technologies demonstrated at Borrego Maneuver Area (BMA) in California. LiDAR data are critical to the overall WAA process in several roles: creation of an accurate high-resolution bare earth digital elevation model (DEM) for ortho-correction of all other remote-sensing datasets; extraction of possible surface munitions related features (MRFs) and for base mapping layers for site visualization, planning and analysis. Orthophotography is valuable for direct detection and visualization of possible MRFs; as input to multiple-sensor fusion algorithms for surface feature detection; and for site visualization and planning.

## **1.2 Objectives of the Demonstration**

The Borrego Military Wash area of the BMA was selected for this study because it is representative of a large number of munitions sites associated with the nearby California-Arizona Maneuver Area and the demonstration was not impeded by limiting site specific characteristics (i.e., vegetation, geology, etc.). The LiDAR and orthophotography demonstration was conducted to determine the utility of these data sets to achieve the following objectives: identification of munitions related features including the two targets identified in the Archive Search Report (ASR); determination of whether evidence exists of any previously unknown target areas; and characterization of site conditions for additional site investigation (i.e., low airborne and ground surveys), planning and remediation.

## **1.3 Regulatory Drivers**

United States Army Corps of Engineers (USACE) is the lead federal agency under the FUDS program. USACE administers the FUDS Military Munitions Response Program (MMRP) program using DoD investigation/cleanup methods based on the U.S. Environmental Protection Agency Comprehensive Environmental, Response, Compensation, and Liability Act (CERCLA) process. Currently the USACE, Los Angeles District, is conducting a Remedial Investigation and Feasibility Study (RI/FS) for munitions and explosives at the former BMA.

The majority of the WAA demonstration site lies within the Anza-Borrego Desert State Park, a unit of the California Parks system. Park personnel were involved in project planning for the WAA demonstration; however, emplacement of ground control target panels for the LiDAR and orthophotography data collection was not allowed on park land, which impacted the spatial accuracy of feature detection results for the demonstration.

## **1.4 Stakeholder/End User**

ESTCP manages the stakeholder issues as part of its WAA-PP. ESTCP uses a process that ensures that the information generated by the demonstration and validation surveys is useful to a broad stakeholder community (e.g., technical project managers and Federal, State, and local governments, as well as other stakeholders).



## 2. Technology Description

### 2.1 Technology Development and Application

Airborne sensors utilized for this demonstration are based on existing, well-developed airborne remote sensing technologies. The data collection, processing and analysis systems used for this demonstration include a fixed-wing plane platform housing the data acquisition technologies and a suite of data processing and analysis software.

#### 2.1.1 Fixed-Wing Platform

The ALTM 3100 LiDAR system, ALTM 4K02 Digital Metric Camera, and the Position and Orientation System (POS) were mounted in the Sky Research Cessna 208 (C208) Caravan aircraft (Figure 1). The C208 is an unpressurized single-engine high wing turboprop with fixed landing gear. A removable composite cargo pod provides housing for the equipment and sensors; both the LiDAR and orthophotography sensors were installed to allow for concurrent data collection.

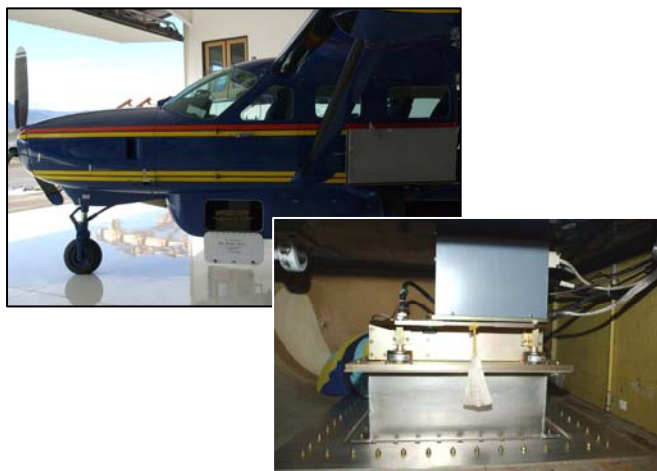


**Figure 1. C208 fixed-wing platform houses the orthophotography and LiDAR sensors for concurrent data collection.**

### 2.1.2 LiDAR System

The LiDAR data collection system – comprised of an Optech ALTM 3100 laser scanner, global positioning system (GPS), and inertial measurement unit (IMU) – is capable of producing precise high-resolution topographic data. The LiDAR sensor specifications are summarized in Table 1 below. For detailed specifications, please see Appendix A.

**Table 1. LiDAR Specifications**

<b>Detector type:</b>	Optech® LiDAR ALTM 3100.
<b>Spacing:</b>	30 centimeters (cm) to 5 meters (m) spot spacing.
<b>Contour Interval:</b>	Dependent on spot spacing with an approximate 1 m (spacing) to 30.5 cm (contour interval) ratio.
<b>Operating Altitude:</b>	80-3,500 m above ground level (AGL) nominal
<b>Elevation Accuracy:</b>	<15 cm at 1200 m; 1 sigma <25 cm at 2000 m; 1 sigma <35 cm at 3000 m; 1 sigma
<b>Horizontal Accuracy:</b>	Better than 1/3,000 x altitude; 1 sigma
<b>Range Accuracy:</b>	2-3 cm, single shot.
<b>Range Resolution:</b>	1 cm
<b>Measurement Rate:</b>	33,000 to 100,000 measurements per second.
<b>Scan Angle:</b>	0 to $\pm 25^\circ$
<b>Swath Width:</b>	Variable from 0 to 0.93 x altitude.
<b>Scan Frequency:</b>	0-70 Hertz (Hz), depending on scan angle
<b>Laser Classification:</b>	Class IV (FDA Code of Federal Regulations (CFR) 21)
<b>Laser Repetition Rate:</b>	33 kilohertz (kHz) (max. altitude above ground level (AGL) 3500 m) 50 kHz (max. altitude (AGL) 2500 m) 70 kHz (max. altitude (AGL) 1700 m) 100 kHz (max. altitude (AGL) 1100 m)
<b>Operating Temperature:</b>	10-35° Celsius (C)
<b>Humidity:</b>	0-95% non-condensing

The laser scanner operates by emitting high-frequency infrared laser beams. The scanner records the time difference between the emission of the laser pulses and the reception of the reflected signal. A mirror mounted in front of the laser rotates, directing the laser pulses to sweep back

and forth perpendicular to the flight direction, which allows the laser scanner to collect swaths of topographic data as the aircraft moves forward. The position of the aircraft is determined by processing differential, dual-frequency, kinematic GPS observations. The GPS located in the aircraft is supported by several ground stations that are located within the vicinity of the acquisition area. The IMU determines the orientation of the aircraft (pitch, roll, and yaw) during data collection. By combining the IMU data with the post-processed GPS data, the exact trajectory of each laser pulse is determined during data processing.

During data acquisition flights, the sensor operator observes the real-time LiDAR swath coverage to assure full coverage of the survey area. The operator also monitors in-flight Position Dilution of Precision (PDOP) and GPS satellite coverage. If tolerance thresholds of either are exceeded, data acquisition activities are put on hold until acceptable conditions resumed. After the data acquisition flights, data from GPS base stations are checked against in-flight GPS data for concurrence. Once data quality assessments are completed, all data (image and ancillary) are transferred to a centralized location for pre-processing and quality control analysis.

### **2.1.3 LiDAR Data Processing**

Processing of the raw data sets employs a variety of software technologies. Sky Research uses the following technologies for processing LiDAR data sets:

- GPS data processing using POSPac/POSGPS® software
- Post-processed GPS data combined with IMU data using POSProc software
- Initial processing and output of LiDAR point cloud data using Optech's REALM software
- Classification of points into vegetation, ground, and "other" was completed in TerraScan software from Terrasolid
- Digital elevation model (DEM) and shaded relief imagery were created from the classified point data using ArcGIS
- Feature Analyst and custom interactive data language (IDL) software algorithms were used to locate, detect, and characterize micro-topographic features, including craters.

### 2.1.4 Orthophotography System

A high-resolution Optech ALTM 4K02 digital metric camera with high-resolution Charged Couple Device (CCD) backing was mounted in the aircraft to capture the aerial photography. This system works as follows: the CCD converts light into electrons, which are enumerated and converted into a digital value. The ability of a CCD to accurately measure and convert the value of electrons into digital format is the measure of quality. As a small format system, the ALTM4K02 camera used for data collection at the site offers a 37 degree field of view minimizing layback distortion at the edges of images. This feature allows for minimal image distortion during the orthorectification phase of processing. The manufacturer's specifications for the Optech ALTM 3100 4K02 digital metric camera used for data collection are summarized in Table 2; detailed specifications are provided in Appendix B.

**Table 2. Camera Specifications**

<b>Detector Type:</b>	OPTECH ALTM 4K02 Digital Metric Camera DSS 301 SN0046- 55 millimeters (mm) lens
<b>Lens Type:</b>	Zeiss Distagon
<b>Focal length:</b>	55.073 mm
<b>Field of View:</b>	36°
<b>CCD Specifications:</b>	4,092 (along flight) x 4,079 (cross flight) Pixel size of 0.000138 inches (in)
<b>Shutter Speed:</b>	1/125 to 1/4000 second
<b>Principal Point</b>	Xppac (mm) -0.390, Accuracy 0.0036 Yppac 0.222, Accuracy 0.0036 Measured from image center (pixel size = 9 microns)
<b>Pixel Non-Squareness</b>	1.0, Accuracy 0.0000001
<b>VIS Calibrated Gain Value</b>	0.98
<b>VIS Calibrated ISO</b>	300
<b>VIS Calibrated Exposure Compensation</b>	-0.70

The camera is linked to a computer or a manual trigger device which controls the frequency and length of exposures, resulting in overlapping images. Information collected from the GPS and IMU are used to rectify the aerial photographs. This is accomplished by assigning a geographic coordinate to each image derived from the processing of the GPS data. In addition, distortions

created by camera tilt, lens distortion, and terrain displacement are removed to produce an orthophotograph.

During the data acquisition flights, the sensor operator observes the real-time photograph footprint coverage to assure required percentage of overlap for the survey area. The operator observes real-time photo display for verification of image quality. The operator also monitors in-flight PDOP and GPS satellite coverage. If tolerance thresholds of either are exceeded, data acquisition activities are put on hold until acceptable conditions resume. After the data acquisition flights, data from GPS base stations are checked against in-flight GPS data for concurrence. Once data quality assessments are completed, all data (image and ancillary) are transferred to a centralized location for pre-processing and quality control.

### **2.1.5 Orthophotography Data Processing**

Sky Research uses the following technologies for processing orthophotography data sets:

- GPS data processing using POSPac/POSGPS® software
- Post-processed GPS data combined with IMU data using POSProc software
- Raw photographs developed into TIFF format with manufacturer-calibrated true-color (VIS) filter
- Images downloaded from removable drives using DSS MissionView 2.0
- Processing of the photographs to sync with GPS data using POSEO 4.1
- ZI Imaging ImageStation Auto Triangulation (ISAT) software was used to combine formatted image files with exterior orientation files
- Aerial photograph rectification to the DTM using ImageStation OrthoPro software.

### **2.1.6 Data Analysis**

Once processed, the LiDAR/orthophotography datasets are analyzed to characterize any MRFs that are visible in the datasets and that may be useful in characterizing munitions contamination present at the site. These surface features may include high-explosive craters, target and range berms, burial trenches, abandoned service roads, artillery targets, and other features where a surface topographic or soil/vegetation expression is observed in the LiDAR and/or orthophotography datasets. Extraction of the potential MRFs from the orthophotography and

LiDAR datasets is both an automated and analyst-performed task that combines multiple-overlay image interpretation with automated spatial feature recognition processes utilizing Environmental Systems Research Institute (ESRI) ArcGIS and Visual Learning Systems' software.

## **2.2 Previous Testing of the Technology**

Component WAA technologies have been developed and tested at a number of defense sites over the past ten years. A WAA at Former Lowry Bombing and Gunnery Range (FLBGR) in Colorado was the first practical application of the use of LiDAR and orthophotography methodology for UXO site assessment. However, at the time the FLBGR WAA was conducted, much of the site had been surface-cleared of munitions contamination at known sites, significantly complicating the analysis.

Since then, demonstrations of LiDAR/orthophotography technologies have been conducted for each demonstration site part of the WAA-PP demonstrations. These results and the contributions of LiDAR and orthophotography technologies are documented in the demonstration reports For each site.

## **2.3 Factors Affecting Cost and Performance**

One of the most important factors affecting performance of airborne remote sensing for wide area assessment is site phenomenology:

- What type of UXO contamination is present at the site?
- What MRFs exist to indicate the presence of contamination?
- What is the degree of correlation between MRFs and contamination?

Regarding cost, for all airborne surveys, the largest single factor affecting the survey costs is the cost of operating the survey aircraft and sensors at the site. These equipment costs are related to capitol value, maintenance overhead and direct operating costs of these expensive sensor and aircraft systems. Mobilization to and from the site increases costs as distance increases, and flexibility of scheduling is critical in determining whether mobilization and deployment costs can

be shared across projects. Another significant cost factor is data volume and the requirement for a robust data processing infrastructure to manage large amounts of digital remote sensing data.

## **2.4 Advantages and Limitations of the Technology**

As with all characterization technologies, site specific advantages and disadvantages exist that dictate the level of success of their application. However, in general, the advantages of high airborne sensor WAA technologies include:

- the ability to characterize very large areas;
- WAA site characterization is defined in terms of MRFs, providing a more robust structure to the overall conceptual site model (CSM);
- ability to deploy multiple sensors to increase the opportunity to define MEC contamination; and
- provide significant “value added” features for site characterization. For example, LiDAR/orthophotography technology provides high fidelity DEMs and high resolution photography within a Geographic Information System (GIS) that can be utilized for a wide variety of site activities.

Limitations of the demonstrated WAA technologies include:

- use of high airborne sensors is not intended to detect individual munitions;
- site physiography, such as terrain and vegetation, can constrain the use of technology for MRF detection;
- LiDAR and orthophotography technologies can only detect MRFs with expression on the earth surface; and
- each technology has survey rate and cost versus detection fidelity trade-offs.

### 3. Demonstration Design

#### 3.1 Performance Objectives

Performance objectives are a critical component of the demonstration plan because they provide the basis for evaluating the performance and costs of the technology. For the LiDAR and orthophotography demonstration at BMA, both primary and secondary performance objectives have been established. Table 3 lists the primary performance objectives for the high airborne remote sensing technology and Table 4 lists the secondary performance objectives, along with criteria and metrics for evaluation.

**Table 3. Primary Performance Objectives**

Type of Performance Objective	Primary Performance Criteria	Expected Performance (Metric)	Performance Confirmation Method
<b>Qualitative</b>	Ease of use and efficiency of operations for each sensor system	Efficiency and ease of use meets design specifications	General observations from project team
<b>Quantitative</b>	Georeference position accuracy for each sensor system	LiDAR: vertical accuracy of 15 cm (5 cm RMSE relative to adjacent sample points); and horizontal accuracy of 40 cm RMSE	Comparison of datasets with ground fiducials*
		Orthophotography: 40 cm RMSE	
	Target Area Detection	>0.98 of target areas having topographic aiming point features	Comparison of ortho and LiDAR data analysis results with ground validation data **

\* Performance confirmation method reported in this table as expected; restrictions on emplacement of aerial targets required revised confirmation method as described in Section 4.

\*\* Original confirmation method reported in this table describes the use of extensive ground validation survey results; instead, a visual site inspection was conducted and used for performance confirmation, as described in Section 4.



**Table 4. Secondary Performance Objectives**

<b>Type of Performance Objective</b>	<b>Primary Performance Criteria</b>	<b>Expected Performance (Metric)</b>	<b>Performance Confirmation Method</b>
<b>Quantitative</b>	Crater Detection	>0.75 (craters < 1m) >0.90 (craters >1 m)	Comparison of LiDAR data analysis results with ground validation data**
	Range Infrastructure Detection	>0.90	Comparison of ortho and LiDAR data analysis results with ground validation data**

*\*\* Original confirmation method reported in this table describes the use of extensive ground validation survey results; instead, a visual site inspection was conducted and used for performance confirmation, as described in Section 4.*

### **3.2 Test Site Selection**

In response to the DSB Task Force report and Congressional interest, ESTCP created the WAA-PP to validate the application of a number of recently developed technologies as a comprehensive approach to WAA. The selection of the former BMA demonstration site as one of several demonstration sites was based on criteria selected by the ESTCP Program Office in coordination with the WAA advisory group of state and federal regulators.

### **3.3 Test Site History/Characteristics**

The Borrego Military Wash is a sub-site of the former BMA, which encompasses approximately 400 square miles (256,000 acres) in eastern San Diego County and western Imperial County, west and southwest of the Salton Sea in California. The former Borrego Maneuver Area comprises desert, mountains, and badlands, with negligible amounts of arid climate vegetation species.

Since site closure, the former BMA lands have consistently been under State, Federal, and private ownership, with the predominant portion used by the State of California as State park

land. The majority of the former BMA lies within the Anza-Borrego Desert State Park, a unit of the California Parks system, and a smaller portion is within the Ocotillo Wells State Vehicular Recreation Area. Usage is expected to remain consistent in the future.

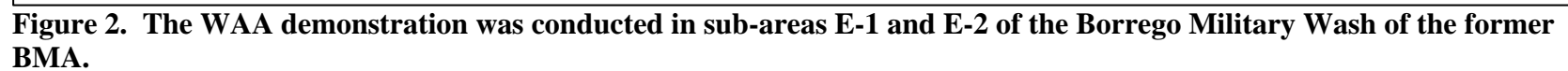
BMA was acquired by use permit from the State of California in 1942 for use as a force-on-force maneuver area. The Army closed their portion in 1944 but the Navy continued to use their areas through 1953. The BMA areas were used to train combat troops for desert warfare, to train mechanized artillery service units and staff, anti-aircraft training, and practice bombing training.

The Borrego Military Wash is located approximately 3 miles due north of the town of Ocotillo Wells and Benson Dry Lake. It contains two sub-areas identified in the ASR. The area designated as E-1 contains a variety of targets and munitions-related features, including contained bombing, strafing, and rocket targets with rake (observation) stations that are firing points for 40mm and 90mm anti-aircraft weapons systems. There also may have been an air-to-ground railway strafing target as well as a bermed area for ground-to-ground firing as part of an Army anti-mechanized target. Sub-area E-2 was designated as a safety buffer area around sub-area E-1.

The Borrego Military Wash 7,940 acre demonstration area was buffered substantially (by 0.5 kilometers [km]) to ensure that all the extents of the project area contained adequate amount of tie points for the orthophotography data set. Figure 2 shows the BMA boundaries, Borrego Military Wash boundaries and the E-1 and E-2 sub-area boundaries. Figure 3 shows the demonstration and data collection boundaries for the LiDAR/orthophotography data collection.

### **3.4 Pre-Demonstration Testing and Analysis**

Prior to data collection flights, a LiDAR calibration flight was completed over a known calibration site located at the Sky Research facility in Ashland, Oregon. This calibration flight served several purposes: to assess the alignment and offsets between the scanning mirror of the sensor, the IMU, and the GPS antenna on the aircraft; and to compare the results of the flight with known survey points. Assessing the alignment and offsets is necessary to ensure that flight lines will not be offset from one another. Comparing the calibration flight results with the known



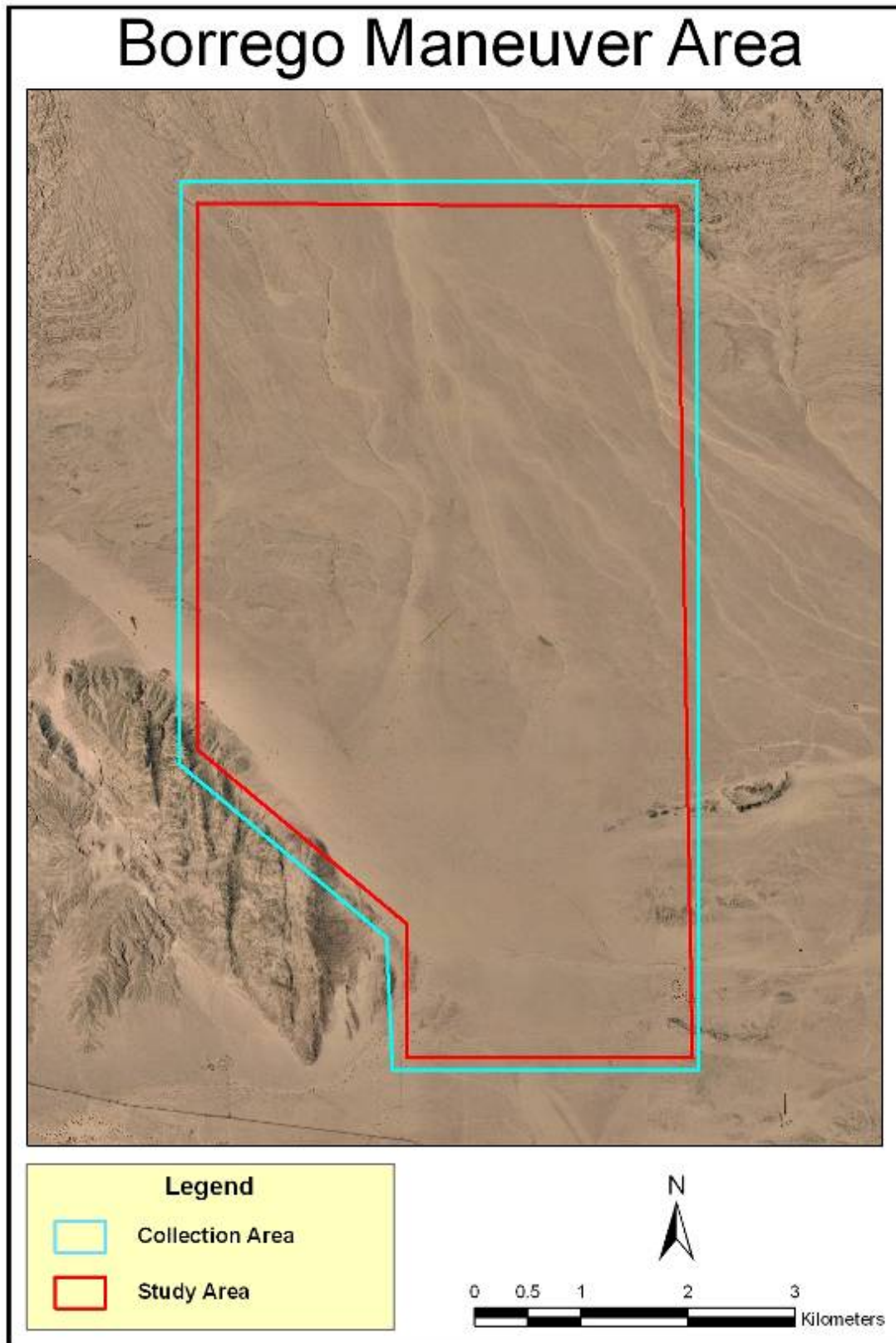


**Figure 3. Collection area and study area boundaries for LiDAR and orthophotography data collection at BMA.**

survey points allows for the calibration of the system to remove all possible offsets. The known survey points used for this comparison are 600 ground control points precisely surveyed on the Ashland airport runway and airport building corners. The second part of the calibration flight included collecting high density LiDAR data over 30 simulated craters. These simulated craters (Figure 4) range in depth from .12 m to .99 m and range in width from .55 m to 2.53 m (Figure 5). Studies on the detection capabilities of the LiDAR sensor to detect the craters in the calibration test plot show a minimal crater detection size of 1.07 m in depth by 0.21 m in width at 500 m AGL. Further information on the craters used for calibration and detection capabilities is provided in Appendix C.

### **3.5 Testing and Evaluation Plan**

#### **3.5.1. Demonstration Set-Up and Start-Up**

Mobilization for this project required mobilization of the plane equipment, pilot, and sensor operators from Ashland, Oregon, and deployment of ground support personnel to establish ground fiducials, establish and operate GPS base stations, and provide logistical support.

#### **3.5.2. Ground Control**

A three-person ground support team operated GPS base stations (Figure 6) and collected GPS road calibration transects. The ground support team included a professional land surveyor to ensure geospatial data accuracy. A survey-grade robotic total station (RTS) was used for precision and efficiency in staking out survey grids and reference datums, in addition to other field positioning tasks.

#### **3.5.3. Navigation Systems**

An Applanix 510 A/V POS system was co-mounted with the LiDAR and orthophotography sensors to record the aircraft's GPS position utilizing a dual frequency GPS receiver and attitude (pitch, roll, and yaw) utilizing an IMU. The Optech ALTM-NAV software package was used for flight navigation. ALTM-NAV allowed the sensor operator to view in real time the swath of the laser system, images taken by the camera, PDOP levels, and number of satellites in the sky, as well as any problems that could have occurred with the laser or camera system. The ALTM-



NAV LED display mounted on the dash of the aircraft allowed the pilots to stay on each flight line within meters to ensure that data gaps did not occur.



**Figure 4.** Example of a calibration site crater with a diameter of 0.75 m and depth of 0.4 m.

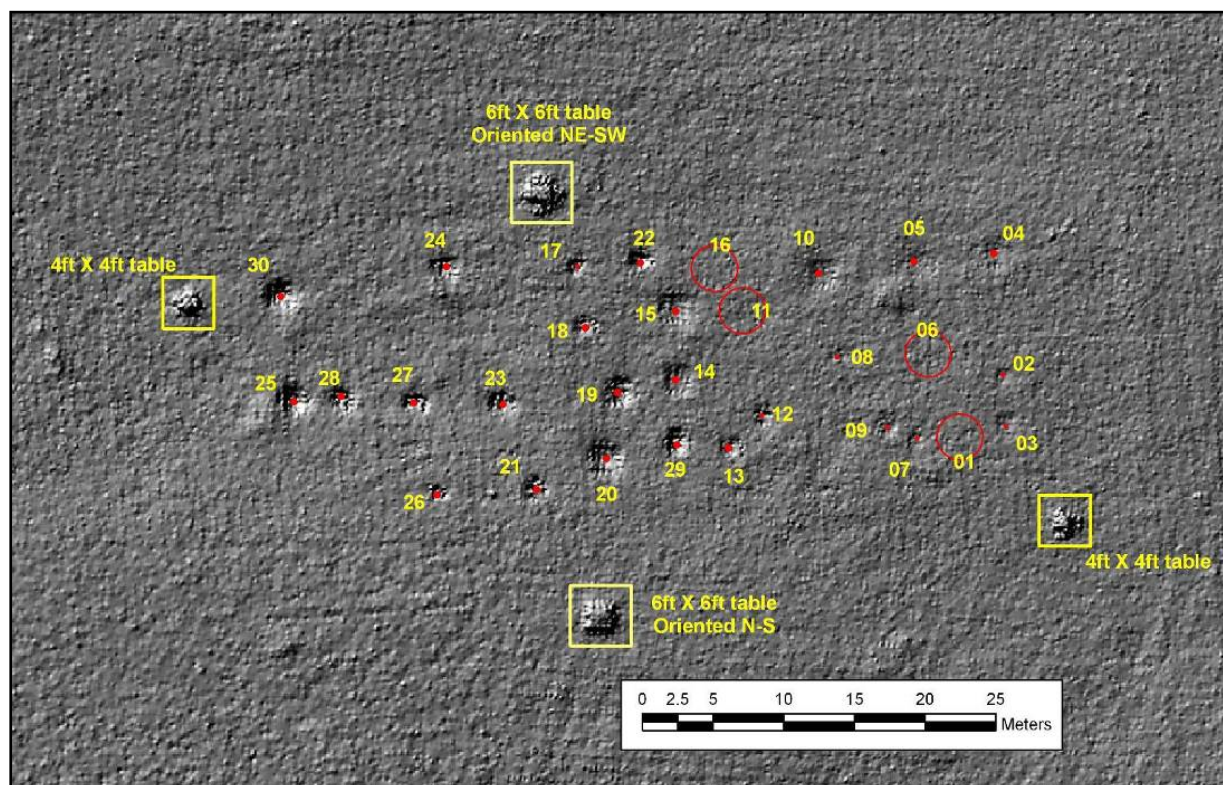


**Figure 5.** Crater calibration area at the Sky Research facility in Ashland, Oregon.

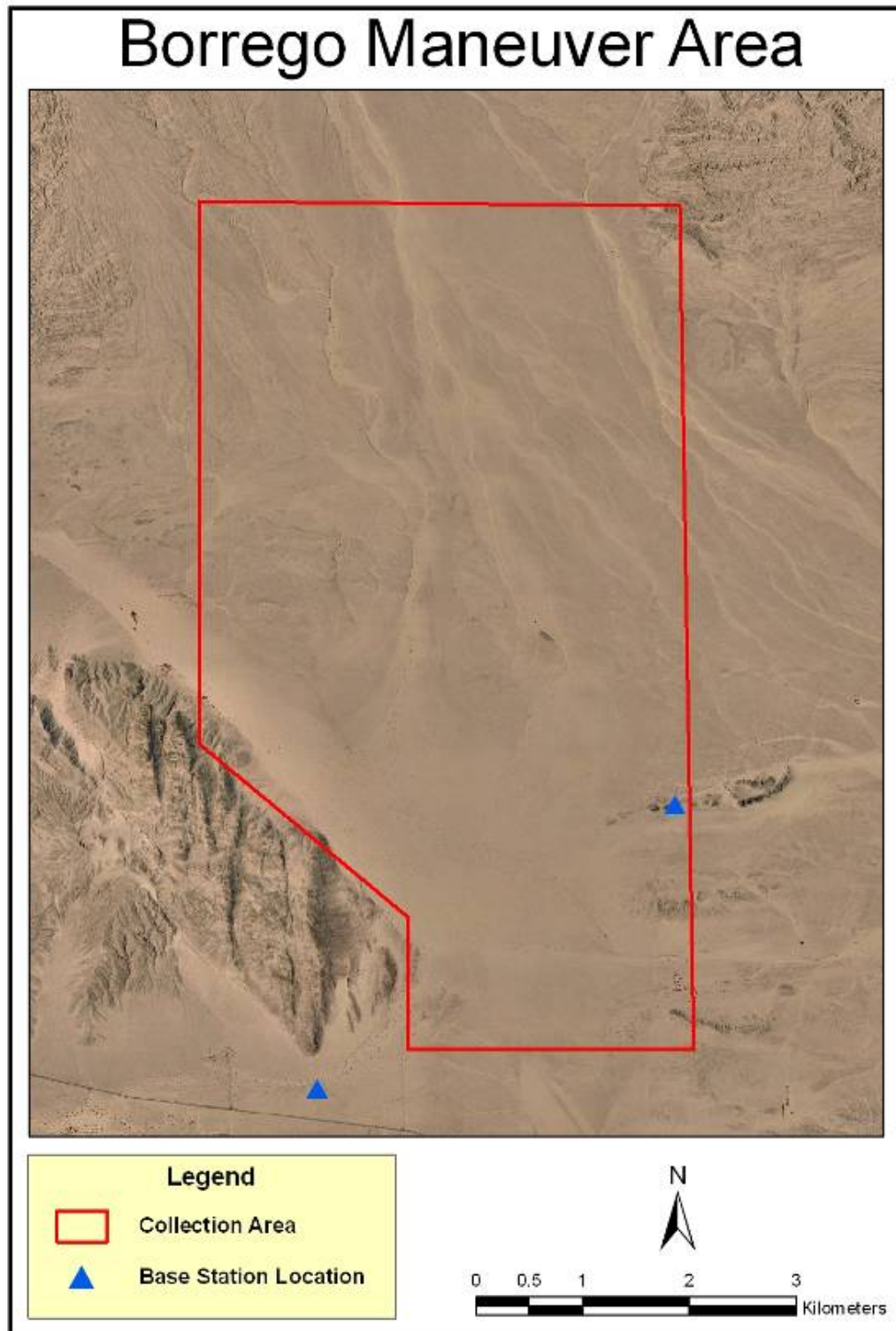


**Figure 6. Location of base stations for high airborne remote sensing data collection at BMA.**

### 3.5.4. Period of Operation

Data collection occurred on August 16, 2005. The data collection included the collection of both LiDAR data and orthophotography for approximately 8,900 acres. The data collection flight took approximately 3.5 hours to complete. The data flight was completed between the hours of 10:00 am and 1:30 pm local time to ensure a good PDOP window, sufficient number of satellites, and sufficiently high sun angles for the photography.

### 3.5.5. Operating Parameters for the Technology

The flight parameters were set to meet the required accuracies and spot spacings at the 800 meters above ground level (AGL) flight altitude used for data collection (Table 5). Flight-line spacing was approximately 230 m to allow a 50% overlap with the 560 m swath width achievable at 800 m. Average elevation sample postings were planned for less than 40 cm, with planned vertical accuracy of 15 cm and horizontal accuracy of 40 cm root mean square error (RMSE). At the planned collection parameters, vertical accuracy relative to adjacent sample points was predicted to be better than 5 cm RMSE, providing very high resolution surface modeling capabilities.

**Table 5. Acquisition Parameters for BMA LiDAR Survey**

<b>Flight Time:</b>	3.5 hours
<b>Flight Altitude:</b>	800 m AGL
<b>Ground Speed:</b>	54 m/second (105 knots)
<b>Measurements per second:</b>	100,000
<b>Scan Width:</b>	370 m
<b>Scan Overlap:</b>	50% (185 m)
<b>Scan Frequency:</b>	60 Hz
<b>Scan Angle:</b>	+/- 13
<b>Spot Spacing:</b>	0.44 m



### **3.5.6. Demobilization**

At the conclusion of the airborne survey, the aircraft and sensor crew demobilized from the site.

## **3.6. Data Processing**

### **3.6.1. LiDAR Data Processing**

LiDAR processing transforms raw binary data into a functional DEM. LiDAR processing was conducted in the following seven steps:

1. **GPS post-processing:** Post-processing of GPS datasets was completed using POSPac/POSGPS® software. Multiple baseline solutions were combined to determine the x,y,z position of the aircraft within 4 inches.
2. **IMU/GPS SBET processing:** The post-processed GPS data were then combined with the IMU data using a processing technique commonly referred to as smoothed best estimate trajectory (SBET) processing. This method combined information about orientation and velocity from the IMU with positioning and velocity information from the GPS data using Kalman filters (the Kalman filter is a data processing algorithm that minimizes mean squared error). The result was a determination of the x,y,z and  $\omega, \kappa, \phi$  parameters for the aircraft at any particular point (position in Universal Transverse Mercator [UTM] 1983 North American Datum [NAD83] meters and the angular orientation of the aircraft). This processing was performed in the proprietary software, POSProc.
3. **LiDAR raw data extraction:** The raw LiDAR data were copied from tape and extracted from the raw data acquisition format into a pre-processed format for output into x,y,z points. Information from the sensor calibration was input into the processing at this point.
4. **LiDAR data calibration:** The variations in altitude and temperatures encountered during normal aircraft operations change the physical characteristics of the LiDAR optics to such a degree that corrections are required. These corrections were completed using manual data calibration techniques created in-house by Sky Research.

5. **LiDAR data output:** Pre-processed LiDAR data were combined with the SBET IMU/GPS data to form the final x,y,z data cloud. This data cloud included all of the returns collected during data acquisition, with each return having an exact x,y,z location.
6. **LiDAR classification:** The x,y,z data cloud were imported into TerraScan LiDAR processing software. Next, the data was classified into point classes. First, all points that were beyond the known elevations of the survey area (known as error points) were removed. The remaining points were then classified automatically and manually into two separate classes: 1) points that represent the ground surface; and 2) all other points that are above the ground surface.
7. **Output data formats:** Key points were used to ortho-rectify the photographs. Surface and bare earth DEM rasters were tiled in ESRI GRID format for loading into the spatial database engine (SDE) geodatabase as a seamless raster, and subsequent derivation of hillshade imagery and other derivative terrain analysis products. Interpolation of LiDAR digital terrain models (DTMs) into DEM rasters was accomplished using Python scripting and the ArcGIS geoprocessing engine.

### 3.6.2. Orthophotography Data Processing

Primary processing of raw digital camera data resulted in a seamless, orthometrically correct 24-bit red-green-blue (RGB) aerial photomap of the site. This true-color imagery was collected and processed to resolve landscape features less than 1 foot across. Sky Research processed orthophotography data in the following steps:

1. **Photo development:** Raw photos were developed into TIFF format with a manufacturer-calibrated true-color (VIS) filter.
2. **GPS post-processing:** Post processing of GPS datasets was performed using POSPac/POSGPS® software. Multiple baseline solutions were combined to determine the x,y,z position of the aircraft within 4 inches.
3. **IMU/GPS SBET processing:** The post-processed GPS data were then combined with the IMU data using SBET. This method combines information about orientation and velocity

from the IMU with positioning and velocity information from the GPS data using Kalman filters. The result was a determination of the x, y, z and  $\omega, \kappa, \phi$  parameters for the aircraft at any particular point (position in UTM NAD83 meters and the angular orientation of the aircraft). Also extracted from this process was an event file documenting the GPS time and POS event identification (ID) for each photograph exposure. This processing was performed in the proprietary software, POSProc.

4. **Camera Photograph ID extraction:** A camera-specific event file was extracted from Camera Mission Folder using DSS Mission View 2.0, containing GPS time and camera photograph ID.
5. **Exterior orientation extraction:** POS photograph event ID and camera photograph ID documents were synced by GPS time and processed in POSEO 4.1. This process incorporated the SBET file with event IDs to create an exterior orientation file assigning x and y center point locations, pitch, roll, and heading to each photograph.
6. **Auto triangulation:** Formatted image files were combined with the exterior orientation file in ISAT software (Figure 7). Tie points were generated automatically using intensity values within designated von Gruber (an automated method for determining tie points within an image) areas. Thirty-six von Gruber areas were assigned per photograph, and approximately eight tie points were generated per von Gruber area. The RMSE for each tie point was calculated using survey control. RMSE and residuals were calculated for all photographs using survey control. Solution for triangulation is accepted when RMSE was less than 1/10,000th of the flying height and residual was less than 1/5,000th of the flying height. Each photo was then adjusted according to individual triangulation results as well as adjusted to the entire data set.
7. **Orthophoto creation:** Triangulation results were loaded into ortho-processing software, along with a LiDAR-derived DTM and aerial photography. Aerial photographs were rectified to the DTM using ImageStation Ortho Pro software. Seam lines were automatically generated based on photo centers then edited for feature consistency. These seam lines designate the point at which multiple photos are to be spliced to form a single mosaic tile (Figure 8). The ortho-corrected photography was then mosaiced into tiles and stored in a geodatabase as a seamless raster.

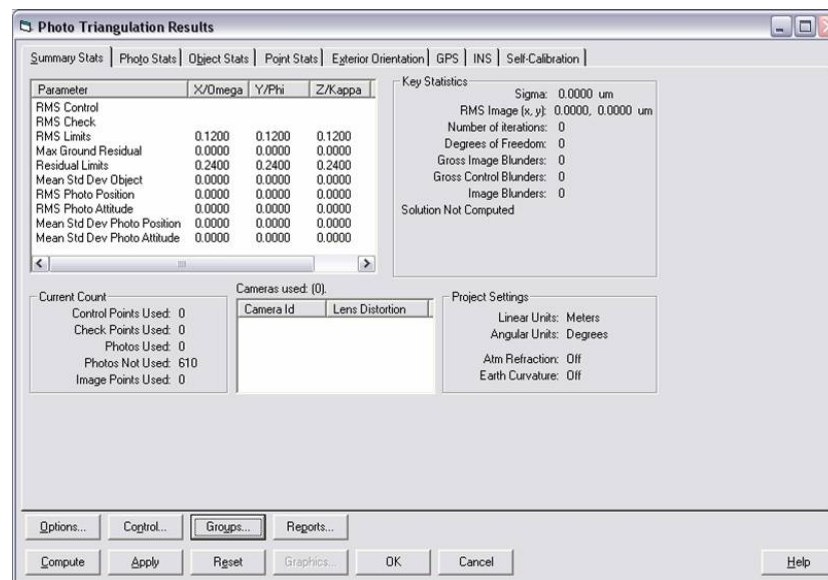


**Figure 7. Screenshot of ISAT aerotriangulation results window.**

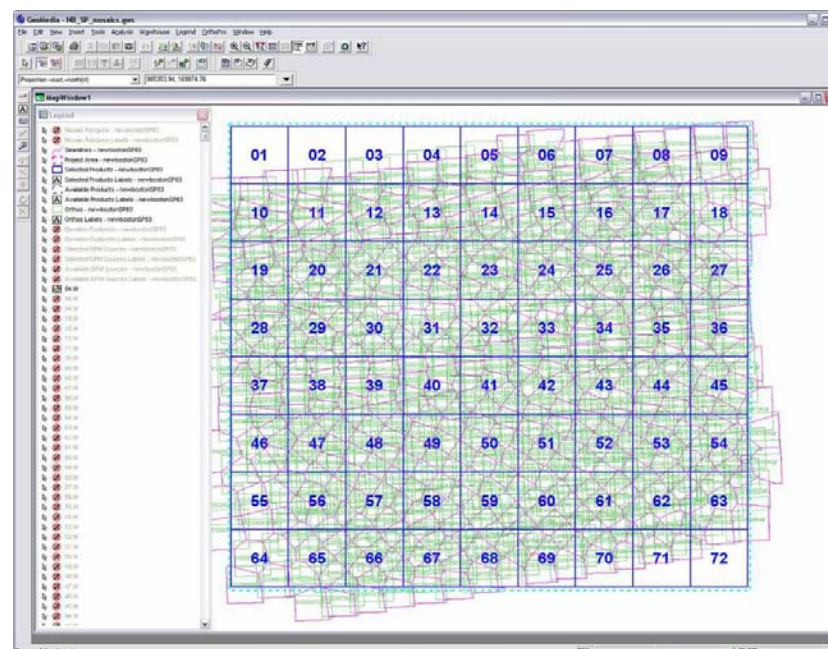


**Figure 8. Screenshot of OrthoPro seam lines (pink), tiles (blue), and photos (green).**

The total size of raw photo data collected amounted to approximately 19.0 gigabytes (GB). This number represents the total number of compressed images as well as navigation data necessary for external orientation processing.

### **3.7. Data Analysis**

Secondary analyses included conversion of processed sensor datasets into suspected munitions-related feature datasets utilizing a variety of processing and analytical techniques. These analyses resulted in feature mapping information from sensor data describing the character and location of probable UXO contamination on the site that could be directly related to historical use data for the site. Detected features were stored in the dataset `FEATURE_OF_INTEREST_CSMV1`.

Several image processing steps were used to generate derivative raster datasets that enhance feature detection, followed by a systematic manual inspection and interpretation of the imagery in a GIS workstation environment that facilitates multiple image overlays with transparency and edge-sweep controls, contrast stretching, multiple-band blending in an RGB color model and other visualization tools, together with the ability to extract interpreted image features into vector point and polygon map features in the geodatabase. The following is a discussion of the general data analytical procedures followed for interpretation of LiDAR and orthophotography datasets.

#### **3.7.1. Computation of Derivative LiDAR Images**

The LiDAR bare earth DEM is used to compute two different derivative images including a “hillshade” image and an “analytic” image. The hillshade is computed using a raster analysis function that computes the hypothetical illumination of a surface by determining illumination values on a cell-by-cell basis for each cell in the image. This is accomplished by defining a vector for a hypothetical light source (azimuth and elevation) and calculating the illumination value for each cell in relation to neighboring cells. A hillshade image is computed for the entire site using a standard `az=315/elev=45` source vector and saved to the geodatabase for performance and consistency, and the operator varies these parameters (and others such as vertical exaggeration) as required to enhance feature visualization. The second derivative “analytic” image is a high-pass filter of the bare earth DEM computed by subtracting the elevation value of each DEM cell from the average of the surrounding cells in a defined circular neighborhood. This process results in an image that emphasizes micro-topographic features in the image of a scale correlated with the filter’s search radius. The neighborhood radius is revised as needed by the operator to enhance visualization of features of various size and shape.

### **3.7.2. Image Analysis Grids**

To enable an efficient and systematic analysis, the study area is subdivided into 100 m grid cells, and each 100 m cell is further subdivided into 20 m cells. This two-tiered grid system is used by the operator to track progress and ensure complete and even review of the imagery as multiple images were overlaid, and examined at various scales and combinations. These analysis grids are quickly generated in ESRI shape file format using standard GIS tools, with attributes to facilitate progress tracking.

### **3.7.3. Target Feature Identification and Extraction**

ESRI ArcGIS Desktop client software environment, the standard operator environment for visualizing, identifying and extracting anthropogenic landscape features qualifying as potential target features, provides visualization tools for revealing and registering underlying image layers, and draping images on the DEM for three dimensional (3D) rendering, for visualization and interpretation of the data. Available datasets within each grid cell are systematically examined for target features including circles, “cross-hair” aiming points, ship outlines, and rectangular shapes that could represent airstrips, buildings, or other target types. As features are identified in an image and corroborated in other imagery, outlines are digitized by the operator into a feature-class geodatabase layer and assigned attributes such as area, centroid, primary and corroborating sensors, description, and feature type, calculated by the remote sensing analyst. Extracted target features are stored in the “Area of Interest” feature class in the geodatabase.

### **3.7.4. Crater Feature Identification and Extraction**

Crater feature identification and extraction utilizes the LiDAR-derived hillshade and analytic high-pass DEM images. For purposes of a crater detection analysis, high explosive (HE) impact craters are defined as circular or semi-circular depressions of any size up to 20 m in diameter. Perimeter circularity, concave bottom profile and raised rim are considered to be diagnostic attributes. To classify a depression as a crater, any significant irregularity of shape (departure from circularity) should be explained by adjacent crater features, rock outcrops, or recent disturbance.

As with target feature extraction, the datasets are analyzed using a systematic manual inspection and interpretation of the imagery in a GIS workstation environment. An automated circular depression detection algorithm is also applied for detecting craters. The automated detection is used to generate candidate detections that were verified or rejected in the manual extraction.

### **3.7.4.1. Automated Crater Detection**

For automated crater detection, the Feature Analyst extension for ArcGIS is used with a custom radial search pattern to generate a preliminary set of topographic depression detections across the study area. Training polygons are established on a variety of obvious crater features identified in the shaded relief imagery, ranging in size from 4 m to 20 m. Four meters is used as the minimum training polygon to minimize the large number of false-detections generated by smaller training shapes. A custom radial search pattern is designed for use by the Feature Analyst spatial classifier that optimized detection of crater-like depressions. The classifier is run directly on the bare earth DEM raster. Once the preliminary depression detections are converted to a polygon GIS feature class, a circularity shape factor is computed for each polygon  $(4 * \pi * \text{Area}) / (\text{perimeter}^2)$ . This shape factor is a type of area/perimeter ratio that results in 1 for a perfect circle and gets smaller as the shape departs from a circle. The circularity attribute is used in the manual extraction of crater features.

### **3.7.4.2. Manual Crater Extraction**

Using the processing grids described above, the operator visually identifies each crater in a grid sector and digitizes a circular feature centered on the center of the crater with the perimeter set to a radius that best follows the rim of the identified crater. Overlapping craters are digitized as overlapping circles. The operator uses the LiDAR shaded relief and analytic high-pass DEM imagery as the basic visualization cue, while the orthophotography is used to support the manual identification by observing vegetation features that respond to altered surface hydrology. The operator uses the automated classification image by setting the circularity threshold and observing the locations of auto-detected depressions to check for any features that may have been missed manually. After the craters are digitized for each analysis grid, the operator runs a custom spatial analysis script within the ArcGIS environment that extracts the high and low elevations within each circle from the underlying DEM, and stores these elevations and the difference (crater depth) as attributes for each. Crater area, perimeter length, and centroid coordinates are also saved as feature attributes. The resulting polygon feature class is saved in the project geodatabase.

### **3.7.4.3. Crater Density Analysis**

To visualize the distribution of craters across the study area, a density analysis is performed by computing a kernel density raster whose cell values each describe the crater density in craters per hectare of a circular neighborhood around each cell. Changes in the neighborhood radius affect the resulting density surface, with larger radii producing a more generalized density model and

smaller radii producing more detail. A neighborhood radius appropriate to the crater density and patterns is interactively determined to produce a density surface most appropriate to the distribution of craters across the study area landscape.

#### **3.7.5. Range Infrastructure Identification and Extraction**

The LiDAR and orthophoto datasets are analyzed to extract other anthropogenic features that can aid interpretation and characterization of the UXO contamination patterns on the site by the spatial correlation of extracted features such as transport routes and evidence of excavation activities with documentary site usage information.

The feature extraction methodology used to extract infrastructure features is essentially the same as that described for the identification and extraction of target features and is conducted concurrently with that extraction. These features are incorporated into the CSM Feature of Interest and Corridors feature classes in the geodatabase and include observed vehicle routes across the study area and locations where the datasets indicate excavation or other grading, fences, utilities, structures, and foundation pads.



## 4. PERFORMANCE ASSESSMENT

### 4.1 Spatial Accuracy

Restrictions on the emplacement of aerial targets precluded the use of a standardized evaluation method for determining spatial accuracy of the datasets; therefore a different approach to estimating spatial accuracy was required to provide estimates of error.

The georeference accuracy of both the orthophoto and LiDAR datasets depended entirely upon the airborne GPS/POS georeferenced data. The rake stations were used to calculate spatial accuracy in the two datasets. The rake stations were used because the eight corners of the two rake stations were clearly delineated in both processed datasets. To use the rake stations for this assessment, the rake station locations were defined in the field by real time kinematic GPS (RTK GPS); the shape of each rake station feature digitized using the hillshade LiDAR image; and the offset between the two calculated. The measured offsets for the eight corners were then averaged to report the estimated accuracies. It should be noted that these estimates do not have measures of variance that provide meaningful information about the confidence error of the estimate since they are associated with a very limited number and scope of measures.

This methodology was used to calculate the mean horizontal offset (89 cm) and the average horizontal offset (22 cm) in the LiDAR dataset and the average horizontal spatial offset (92 cm) of the orthophotography dataset (Table 6).

**Table 6. LiDAR and Orthophotography Data Accuracy Results**

<b>Dataset</b>	<b>Accuracy Metrics</b>	<b>Results (in cm)</b>
LiDAR	RMSE Vertical Linear Error (68.3% confidence level)	62
LiDAR	Vertical Linear Error (95% confidence level)	22
LiDAR	Horizontal Accuracy Estimate	89
Orthophotography	Horizontal Accuracy Estimate	92

## **4.2 Data Analysis Results**

During the analytical phase of this demonstration, a total of five features were detected in the combined datasets: one target circle and a railroad strafing target classified as target areas; and two rake stations and a small depression possibly consistent with munitions related activity classified as range infrastructure (Figure 9). No craters were detected in either dataset.

### **4.2.1 Target Area Detection**

The results of the target feature analysis for BMA included a determination of the exact size and location of the Bomb Target 64 (BT64) target circles, a vehicle target and railroad strafing targets. In addition, there is evidence to support the conclusion that the rake stations were also used as targets, and therefore they are included as targets that were detected in the data.

The target circles for BT64 were located in a minor topographic basin lying in an upland dividing the main branches of the Borrego Military Wash which bisects the study area and approximately 1000 feet to the east-southeast of the “target center” location point provided in the ASR. The BT64 target feature consisted of three concentric circles approximately 75’, 150’, and 300’ in diameter (Figure 10). These features were constructed by flat-grading the pattern in lines approximately 5 m wide, resulting in minor (generally less than 0.5 m below adjacent surfaces) circular depressions with small ridges along the edge of each. These features are best-defined in the orthophotography from the vegetation pattern which has emerged on the small ridges, and can also be discriminated in the LiDAR analytic image.

The railroad strafing target was located approximately 2000’ to the southeast of the “mile long wooden track” location point provided in the ASR in the same topographic basin where BT64 is located. This feature is a raised berm less than 0.5 m high and about 2500’ long (about 0.5 miles), running east to west (Figure 11). This feature was constructed by grading a raised berm in the configuration of a typical railroad bed. This feature is well-defined in the orthophotography, LiDAR hillshade, and analytic high-pass LiDAR images. Ground support field observations at this location included burned fragments of milled wood and very high densities of box nails

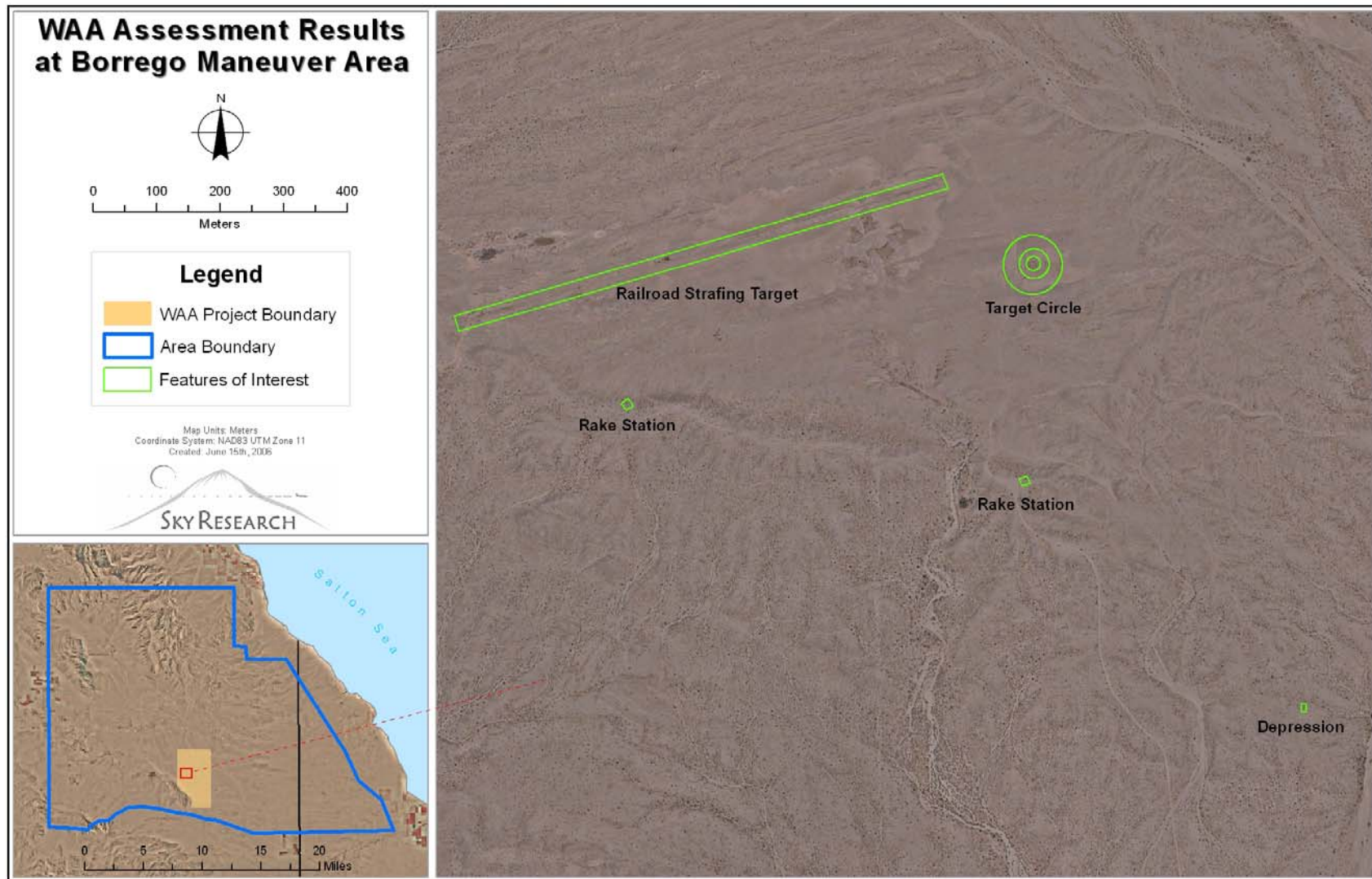
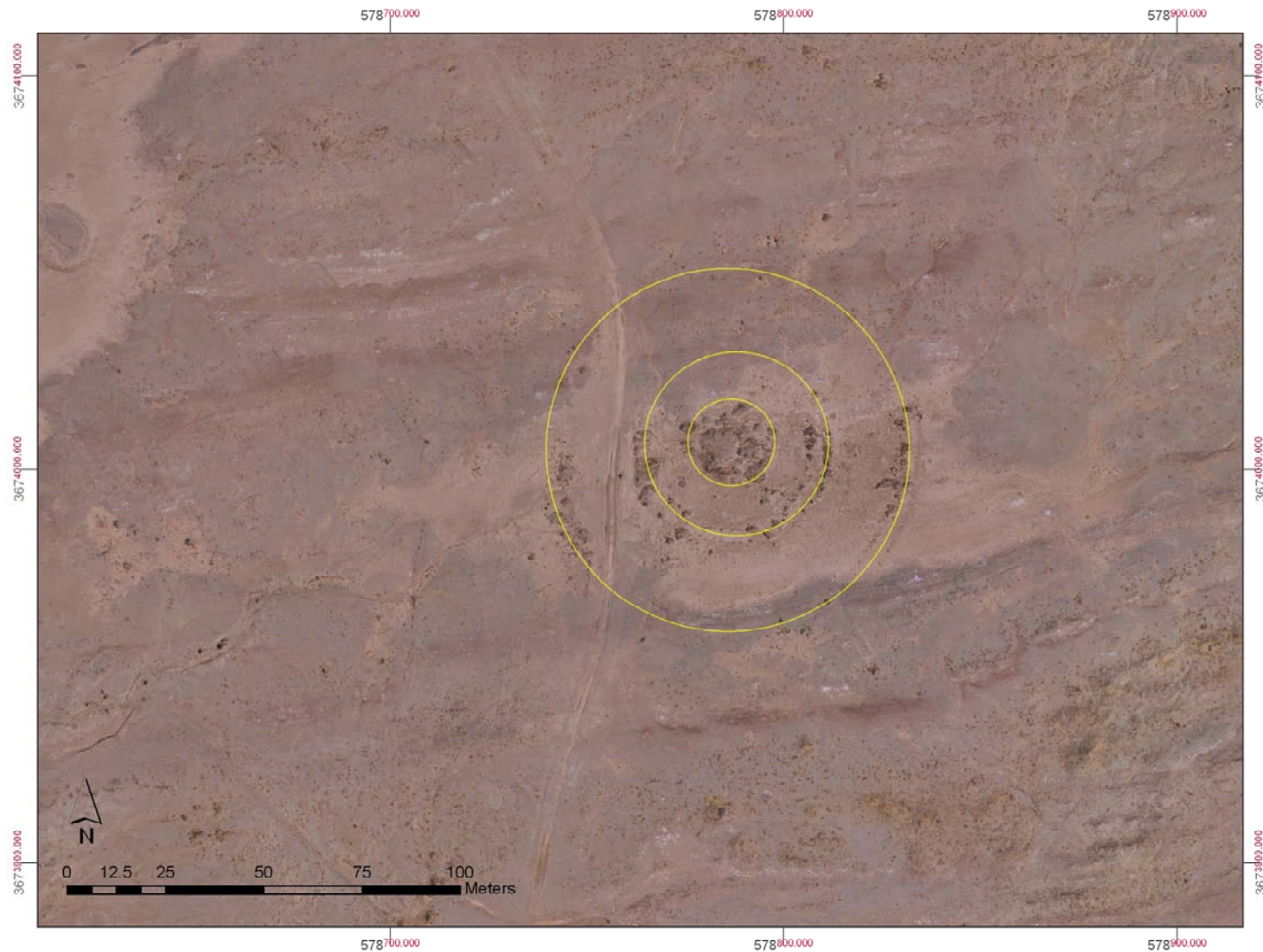
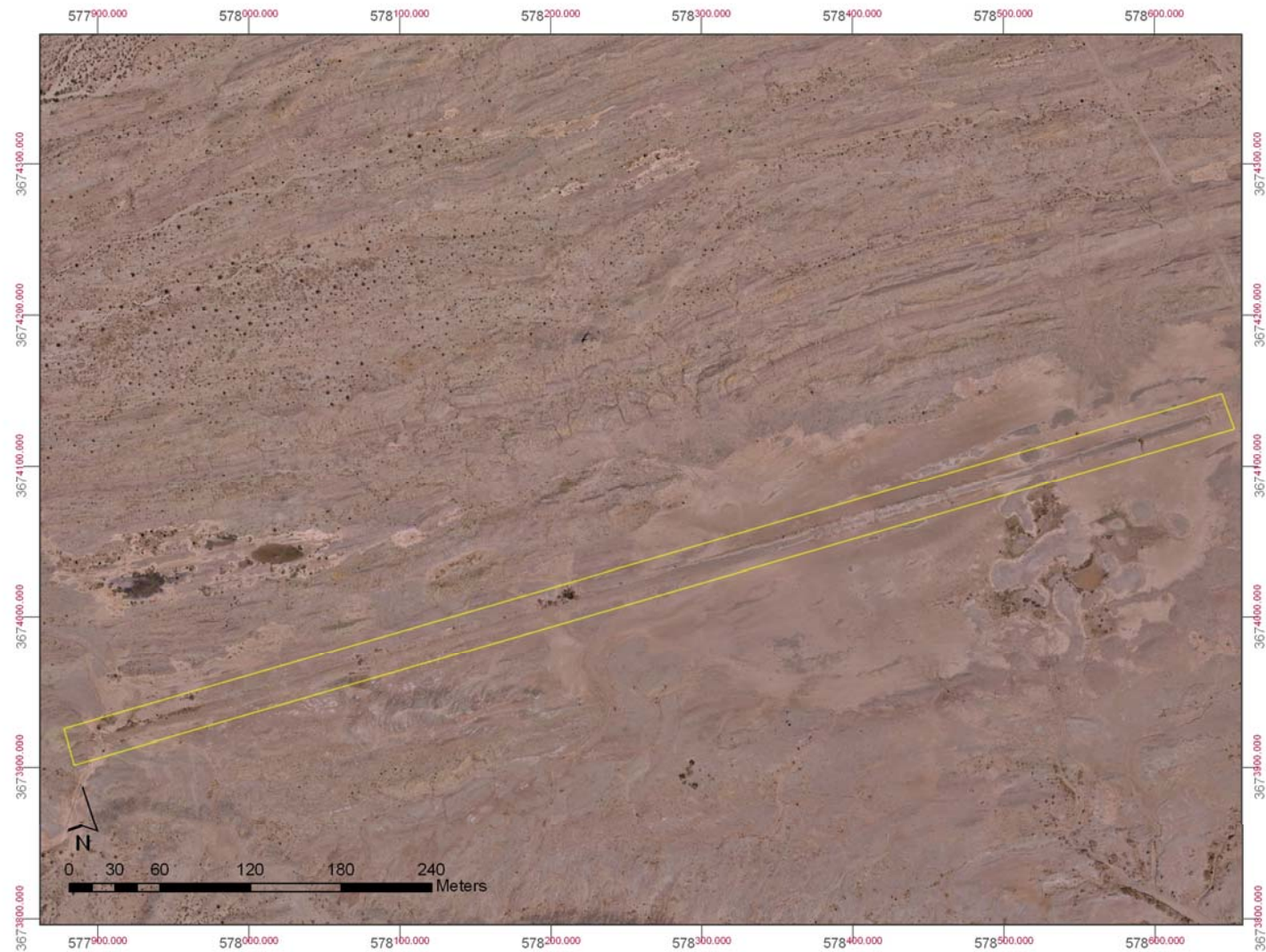


Figure 9. Munitions related features detected at BMA utilizing high airborne orthophotography and LiDAR datasets.



**Figure 10. Extracted circular aiming point target features for BT64 shown on color orthophoto.**





**Figure 11. Extracted railroad strafing target shown on the color orthophoto image.**

consistent with the ASR information that the railroad strafing target included wooden targets constructed from wooden munitions crates.

Although several bullet-ridden vehicle targets were observed by ground crew prior to and during data collection activities and were also observable in the orthophotography (with prior knowledge concerning where to look), they were not detected during the independent feature detection process. It is postulated that if the metal distribution models derived from low airborne geophysical surveys were available to use as a training set for analysis, these features could have been detected and mapped.

#### **4.2.2 Crater Detection**

No HE craters were detected in the vicinity of BT64 or elsewhere in the demonstration area. This result is not surprising since no HE aerial bombs had been documented in use at the site, and the only documented HE munitions were 5" high velocity air rockets (HVAR) that normally carried a relatively small (7 pounds of Trinitrotoluene [TNT]) HE charge.

#### **4.2.3 Range Infrastructure Detection**

Two rake stations and a small depression were identified during data analysis. Positions for both rake stations were determined from the orthophoto imagery. The western rake station was located approximately 400 m northeast of the location provided in the ASR, and the eastern rake station was located approximately 330 m northwest of the ASR location. Both locations are situated on high ground looking northwards down into the area where BT64 and the railroad strafing target are located, and each have a clear view of both target features. Transport features mapped include the access road through the site which is currently in active use by park visitors. This road accesses both the eastern rake station and BT64. Figure 12 shows large-scale views of the two rake stations.

A small depression was also identified in the data analysis, (Figure 13). After review, this depression was selected as a feature of interest.

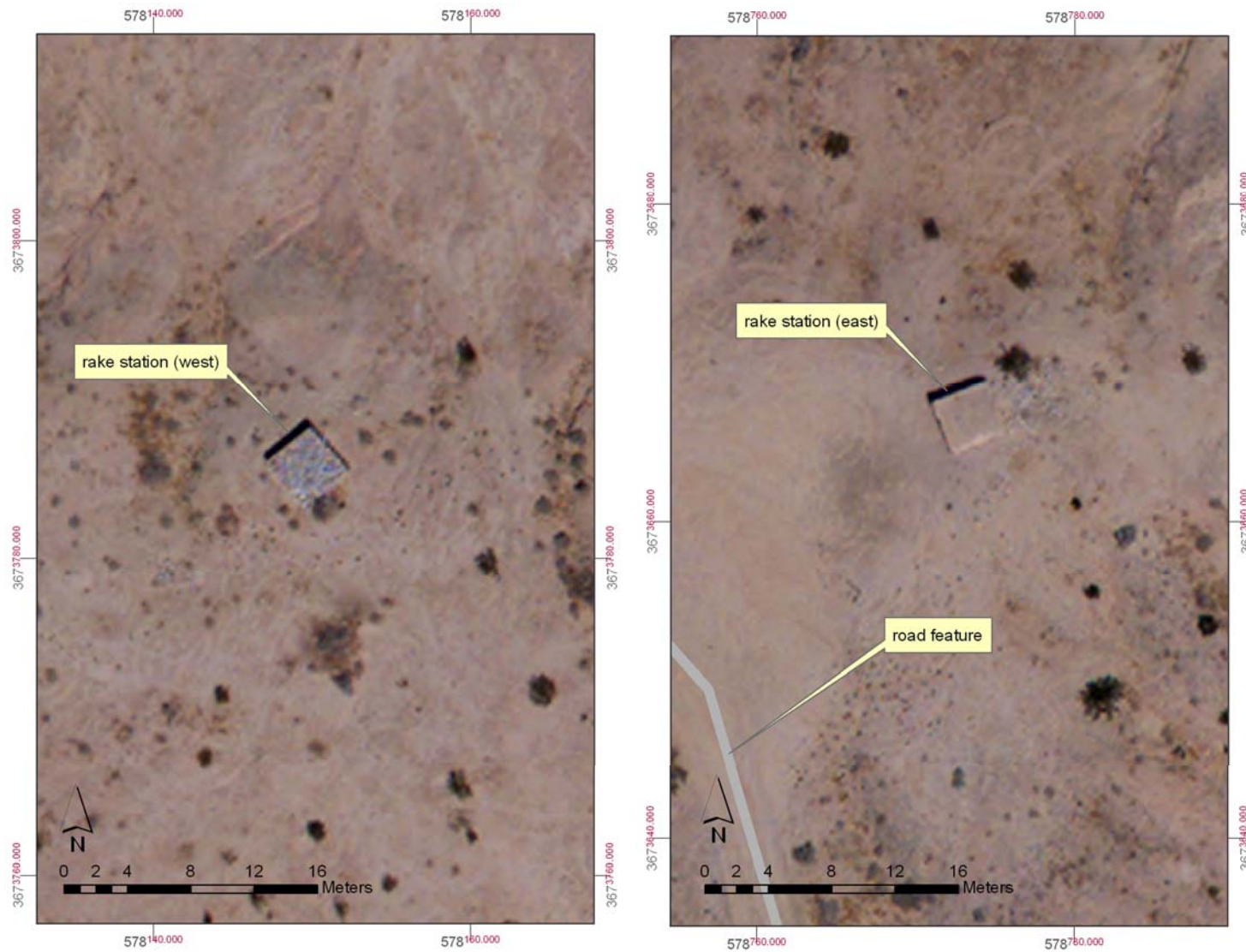
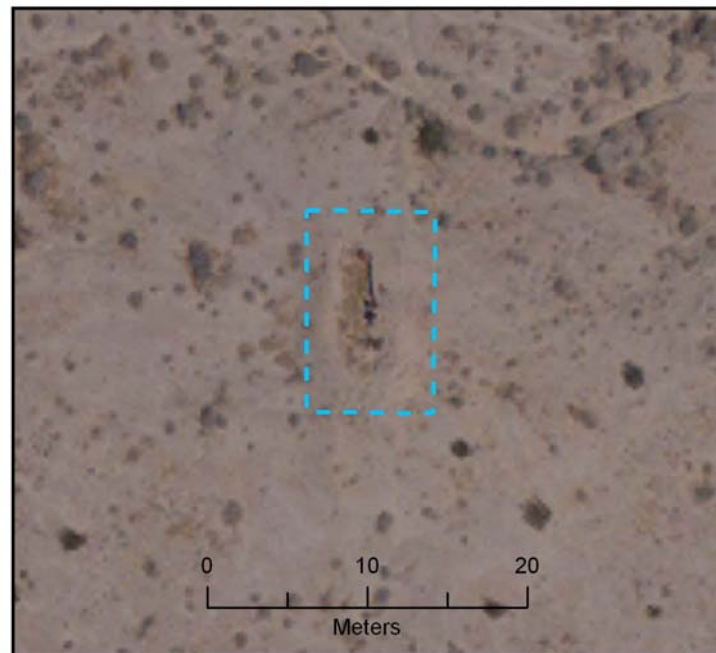


Figure 12. Large-scale views of the rake station range infrastructure features.



**Figure 13. Small depression detected in data and identified as a feature of interest.**

### 4.3 Performance Criteria

The performance of the high airborne remote sensing technologies was measured against the criteria listed in Table 7.

**Table 7. Performance Criteria**

Performance Criteria	Description	Type of Performance Objective
Ease of use and efficiency of operations for each sensor system	Efficiency and ease of use meets design specifications	Primary/Qualitative
Georeference position accuracy for each sensor system:	Calculated from average offset for eight corners of two rake stations.	Primary/Quantitative
Target Area Detection	Comparison of ortho and LiDAR data analysis results with site visit data.	Primary/Quantitative
Crater Detection	Comparison of LiDAR data analysis results with site visit data.	Secondary/Quantitative
Range Infrastructure Detection	Comparison of ortho and LiDAR data analysis results with site visit data.	Secondary/Quantitative



#### 4.4 Performance Confirmation Methods

Table 8 details the confirmation methods that were used for each criterion, the expected performance and the performance achieved.

**Table 8. Performance Confirmation Methods and Results**

Performance Metric	Confirmation Method	Expected Performance	Performance Achieved
Technology Usage	Field experience using technology during demonstration	Efficiency and ease of use meets design specifications.	Pass
Georeference accuracy	Calculated from average offset for eight corners of two rake stations.	LiDAR: vertical accuracy of 15 cm (5 cm RMSE relative to adjacent sample points); and horizontal accuracy of 40 cm RMSE	Vertical Accuracy: 62 cm (22 cm relative to adjacent sample points); estimated horizontal accuracy of 89 cm
		Orthophotography: 40 cm RMSE	92 cm RMSE
Target Area Detection	Comparison of ortho and LiDAR data analysis results with site visit data	>0.98	0.83 5 target features detected ( target circle, railroad strafing target, 2 rake stations, and small depression); 1 target feature not detected
Crater Detection	Comparison of LiDAR data analysis results with site visit data.	>0.75 (craters >1m) >0.90 (craters <1 m)	N/A, no craters detected, none found during visual reconnaissance
Range Infrastructure Detection	Comparison of ortho and LiDAR datasets with site visit data.	>0.90	Identified features verified as range infrastructure

#### **4.4.1 Technology Usage**

The use of LiDAR and orthophotography in a high airborne, fixed-wing aircraft is an efficient means for collecting data over large survey areas. The LiDAR sensor and digital camera utilized for this demonstration are easy to operate. The standardized data processing and analysis methodologies are well understood and easy to use for experienced remote sensing analysts.

#### **4.4.2 Georeference Accuracy**

The georeference accuracy achieved for this demonstration was affected by the restriction on emplacing aerial targets. Typically, emplaced aerial targets are used for calibrating and georegistering LiDAR and orthophotography processed data, while some targets are normally reserved for accuracy assessment (i.e. not used in processing). Because reference targets were not available within the survey image area for processing, the georeference accuracy of both the orthophoto and LiDAR datasets depended entirely upon the airborne GPS/POS georeferenced data. Consequently, the final image accuracy was significantly degraded relative to expected accuracies as shown in Table 9. For accuracy assessment of both the LiDAR and orthophoto datasets, the rake stations corners were defined in the field by RTK GPS and compared to digitized locations visible in both processed datasets. The rake station corner coordinates could not be used as ground reference points to refine the data georegistration in place of the independent aerial targets normally used because using these features for both calibration and accuracy assessment would have artificially reduced the computed positional error.

While the georeference accuracies specified in the demonstration design were not met for this demonstration due to the lack of adequate ground control, the level of accuracy was considered to be adequate for reacquisition of these identified features in the field and for all generalized feature mapping requirements at the site.

#### **4.4.3 Target Area Detection**

Post-analysis verification ground surveys identified the presence of munitions in six areas presumably used as targets: two target circles, linear railroad strafing target, the two rake stations, and the small depression.

The ground surveys identified the circular outline of circular bombing target defined by multiple concentric circular vegetation patterns on mostly eroded earthen berms (Figure 14), which was detected in both the LiDAR and orthophotography datasets. This area was characterized by extensive practice bomb munitions scrap (Figure 15).



**Figure 14. Outline of target circles as photographed during visual reconnaissance survey.**



**Figure 15. 100 lb bomb scrap as photographed in target circle during visual reconnaissance survey.**

Ground surveys confirmed the presence and location of the railroad strafing target identified in both the LiDAR and orthophotography datasets. The ground surveys described this feature as a 20' wide raised straight railbed, slightly higher in the center than at the edges. While no steel rails or ties were located, thousands of nails and burned wood were found, which is consistent with the ASR description of the strafing target's construction from wooden ammunition crates.

A small depression detected in the data analysis was found to be a small depression in the ground, with a partially buried target still evident (Figure 16). Munitions scrap (50 cal and 20 mm) were found in this area (Figure 17).



**Figure 16. Partially buried target in small depression detected during data analysis.**



**Figure 17. Munitions scrap found in small depression area.**



Ground survey results indicate that the rake stations were used as targets as well as observation posts, as munitions debris, including 20 mm and 100 lb bomb scraps, were found in and around the rake stations during the survey (Figures 18 and 19). Therefore, the rake stations were used in calculation of the performance of the datasets in detecting target areas as well as detection of range infrastructure.



**Figure 18. Concrete rake station.**



**Figure 19. 20 mm located in concrete of rake station.**

The overall performance of the technologies did not meet the expected performance criteria as a second target circle was not detected. This target circle was located during the ground surveys south of the strafing target and west of the previously mentioned target circles. This second target circle is defined by widely spaced scattered rock piles aligned in a circular pattern. These rocks were too small to be delineated from the underlying terrain in either the LiDAR or the orthophoto datasets. The Borrego site was selected because the erosional and depositional conditions of blowing sand and periodic flooding represent significant challenges to munitions-related feature detection. The point of this exercise was to determine to what degree LIDAR is a viable technology in these conditions. It is clear from our analysis that while we are capable of identifying munitions related features at Borrego, false negatives are possible in this kind of environment.

#### **4.4.4 Crater Detection**

While some evidence of high explosive munitions use at the site was presented in the ASM, no detonation craters were detected during the data analysis and no craters were identified during the visual reconnaissance survey. This is consistent with the smaller HE munitions used (rockets), and degree of wind and water erosion evidenced by the other features identified. The railroad berm appeared to be significantly eroded from its original configuration, and the eastern target circle was identified only by the pattern of vegetation which originally grew on the now mostly eroded berm.

#### **4.4.5 Range Infrastructure Detection**

Both concrete rake stations identified during the data analysis were located and verified during the visual survey (Figure 18).

### **4.5 Performance Assessment Summary**

The Borrego site presented a number of interesting new challenges to WAA technologies and methods based on a foundation of high resolution LiDAR and orthophoto datasets. First, environmental considerations required that ground-disturbing fiducials and aerial targets not be used. This led to a reduction in geospatial data accuracy, with an approximate doubling of horizontal and vertical error over data acquired and processed using ground target reference points. However, the munitions features that were identified were geolocated with sufficient

accuracy to allow easy acquisition in the field and represented a significant increase in accuracy over the locations provided in the ASR.

Second, the part of the study area containing the main target features was subject to water erosion and periodic flooding and wind erosion and deposition, with significant reduction in the ability to observe man-made terrain features such as target berms and detonation craters. However, one of the two aiming circles was still detected from vegetation changes related to the mostly eroded target berms and the railroad strafing target was still clearly delineated in spite of significant erosion reduction. Although HE munitions were apparently used at the site based on information in the ASR, no detonation craters were detected. This is probably due to wind and water erosion and deposition. This points out the importance of environmental factors, including both natural and man-caused disturbance, in the preservation and detection of munitions related features with WAA technologies.

Finally, this site qualifies the generalization that arid desert and high plains munitions sites are uniformly well preserved from natural disturbance and amenable to remote sensing feature detection methods. Soils, hydrology, climate, and human disturbance factors need to be carefully considered for each prospective WAA site in order to understand the probable persistence of features over time and the likelihood of detection for various types of munitions related features.

## 5. Cost Assessment

### 5.1 Cost Reporting

Cost information associated with the demonstration of all airborne technology, as well as associated activities, were tracked and documented before, during, and after the demonstration to provide a basis for determination of the operational costs associated with this technology. For this demonstration, Table 9 contains the cost elements that were tracked and documented for this demonstration. These costs include both operational and capital costs associated with the demonstration design and planning; salary and travel costs for support staff; equipment costs associated with aircraft, sensor and camera, support personnel, and costs associated with the processing, analysis, and interpretation of the results generated by this demonstration.

**Table 9. Cost Tracking**

<b>Cost Category</b>	<b>Sub Category</b>	<b>Details</b>	<b>Costs (\$)</b>
<b>Start-Up Costs</b>	Pre-Deployment and Planning	Includes planning, contracting, site visit and site inspection	\$5,545
	Mobilization	Personnel mobilization, equipment mobilization, and transportation	\$10,050
<b>Operating Costs</b>	High Airborne Survey	Data acquisition and associated tasks, including aircraft operation time	\$17,707
<b>Demobilization</b>	Demobilization	Demobilization	\$6,178
<b>Data Processing and Analysis</b>	Data Processing & Analysis	Processing and analysis of LiDAR and orthophotography data	\$11,400
<b>Management</b>	Management and Reporting	Project related management, reporting and contracting	\$15,405
<b>Total Costs</b>			\$66,285
<b>Acres Surveyed</b>			7,940
<b>Unit Cost</b>			\$8.35/acre



## **5.2 Cost Analysis**

A major cost driver for an airborne survey system is the cost of aircraft airtime. In terms of tasks, this constitutes a large percentage of the mobilization, data acquisition and demobilization costs. Mobilization and demobilization costs are generally a function of the distance from the home base for the aircraft, equipment and personnel. For this demonstration, the aircraft mobilized and demobilized between Ashland, Oregon, and the demonstration site, requiring on average 4 hours of flight time in each direction.

In addition, the cost of equipment (LiDAR sensor, digital camera and GPS equipment constituted a large percentage of the data acquisition costs for this demonstration. Data processing and analysis functions made up the bulk of the remaining costs associated with the results of the demonstration.

Project management and reporting were a significant cost for this demonstration, as the project was conducted under the WAA-PP and required more meetings, travel and reporting than would generally be expected for a production level survey.

Costs associated with validation were not considered in the cost analysis, as the validation was conducted as part of the WAA-PP.

## **6. Implementation Issues**

### **6.1 Regulatory and End-User Issues**

The ESTCP Program Office has established a WAA-PP Advisory Group to facilitate interactions with the regulatory community and potential end-users of this technology. Members of the Advisory Group include representatives of the US EPA, State regulators, Corps of Engineers officials, and representatives from the services. ESTCP staff have worked with the Advisory Group to define goals for the WAA-PP and develop Project Quality Objectives.

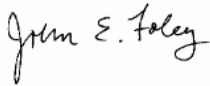
There will be a number of issues to be overcome to allow implementation of WAA beyond the pilot program. Most central is the change in mindset that will be required if the goals of WAA extend from delineating target areas to collecting data that are useful in making decisions about areas where there is not indication of munitions use. A main challenge of the WAA-PP is to collect sufficient data and perform sufficient evaluation that the applicability of these technologies to uncontaminated land and their limitations are well understood and documents. Similarly, demonstrating that WAA data can be used to provide information on target areas regarding boundaries, density and types of munitions to be used for prioritization, cost estimation and planning will require that the error and uncertainties in these parameters are well documented in the program.

## 7. Points of Contact

**Table 10. Points of Contact**

Point of Contact	Organization	Phone/Fax/email	Role in Project
Dr. John Foley	Sky Research, Inc. 445 Dead Indian Road Ashland, OR 97520	(Tel) 978.479.9519 (Fax) 720.293.9666	Principal Investigator
Ms. Stacey Kingsbury	Sky Research, Inc. 445 Dead Indian Road Ashland, OR 97520	(Tel) 540.961.9132 (Fax)	Project Manager
Mr. Jerry Hodgson	USACE Omaha District 215 N. 17 <sup>th</sup> Street Omaha, NE 68102-4978	(Tel) 402.221.7709 (Fax) 402.221.7838	Federal Advocate
Mr. Hollis (Jay) Bennett	US Army R&D Center (CEERD-EE-C) 3909 Halls Ferry Road Vicksburg, MS 39180-6199	(Tel) 601.634.3924	DoD Service Liaison

Project Lead Signature:



## Appendix A: Optech ALTM 3100 Specifications

**ALTM 3100: 3,500 m altitude! 100,000 laser pulses per second!**

### ALTM 3100 Specifications

#### Airborne Module

Operating altitude	80 - 3,500 m nominal
Horizontal accuracy	1/2,000 x altitude; 1 sigma
Elevation accuracy	<15 cm at 1.2 km; 1 sigma <25 cm at 2.0 km; 1 sigma <35 cm at 3.0 km; 1 sigma
Range resolution	1 cm
Range capture	Up to 4 range measurements for each pulse including last
Intensity capture	12 bit dynamic range for each measurement
Scan frequency	Variable; maximum 70 Hz
Scan angle	Variable from 0 to $\pm 25^\circ$ , in increments of $\pm 1^\circ$
Scanner Product	Scan angle x scan frequency $\leq 1,000$
Roll compensation	5 Hz update rate (Scan angle + Roll comp. angle = $25^\circ$ , i.e., $\pm 20^\circ$ scan allows $\pm 5^\circ$ compensation)
Swath width	Variable from 0 to $0.93 \times$ altitude m
Position Orientation System	Applanix - POSAV 510 including Internal 12 channel dual frequency 2 Hz GPS receiver
Spot distribution	Sawtooth, uniform across 96% of scan
Laser repetition rate	33 kHz (max. altitude (AGL) 3.5 km) 50 kHz (max. altitude (AGL) 2.5 km) 70 kHz (max. altitude (AGL) 1.7 km) 100 kHz (max. altitude (AGL) 1.1 km)
Data storage hard drives	Ruggedized removable hard drive Minimum 7 hr. continuous log time @ 100 kHz
Beam divergence	Dual divergence 0.3 mrad (1/e) or 0.8 mrad (1/e)
Laser classification	Class IV (FDA CFR 21)
Power requirements	28 VDC, 35 A (maximum)
Operating temperature (air temperature)	Control rack: $+10^\circ\text{C}$ to $+35^\circ\text{C}$ Sensor head: $-10^\circ\text{C}$ to $+35^\circ\text{C}$ (assuming the use of thermal jacket)
Storage temperature	$-10^\circ\text{C}$ to $+50^\circ\text{C}$
Humidity	0 - 95% non-condensing



#### Control Rack

Vibration-isolated case:	
Dimensions/weight (in-flight)	65 cm x 59 cm x 49 cm/53.2 kg covers removed, with removable hard drive installed
Cables/laptop	7.6 kg/3 kg

#### Sensor Head

Fits standard camera mounts or mounts directly to floor	
Overall dimensions/weight (in-flight)	26 cm x 19 cm x 57 cm/23.4 kg (incl. sensor insulating jacket)
Minimum opening	19.2 cm x 25.5 cm (flight direction)

#### Processing Software

REALM Survey Suite	Differential kinematic GPS solution Trajectory optimization from multiple base stations XYZ point calculations module Vegetation classification/extraction feature Windows NT/2000/XP compatible
--------------------	--

#### GPS Ground Support

Multiple base stations	Any dual frequency receiver with Rinex output
------------------------	---

#### Available Options

4k x 4k Digital camera	Integrated metric frame camera to deliver geo-referenced (X,Y,Z) color or color-IR images with sub-pixel accuracy
Intelligent Waveform Digitizer	8 bits @ 1 nsec sample interval per pulse (maximum 50 kHz)

Note: to meet its stated accuracy, the ALTM must receive GPS data of sufficient quality. GPS data quality shall be viable only when all of the following conditions are met:

- At least four satellites are in lock (tracked by the receiver) throughout the survey
- Elevation of the satellites is good (i.e., PDOP < 4)
- Aircraft stays within 30 km of the GPS base station

If one or more of these conditions is not met, or if any source of electromagnetic interference causes the GPS receivers to repeatedly lose lock, the specified accuracy of the ALTM will be compromised.

Specifications subject to change without notice.

100 Wildcat Road • Toronto, ON • Canada M3J 2Z9

Tel: [416] 661-5904 • Fax: [416] 661-4168

Web: [www.optech.on.ca](http://www.optech.on.ca) • Email: [inquiries@optech.on.ca](mailto:inquiries@optech.on.ca)

© Copyright 2004, Optech Incorporated. All rights reserved. 270104



## Appendix B: ALTM 4K X 4K Digital Camera Specifications

### ALTM 4K02 - The Digital Image Collection and Processing Solution

#### Specifications

##### Camera

Array size	4,092 (along flight) x 4,079 (cross flight) pixels
Pixel size	0.009 mm
Premium grade CCD*	Point defects <= 2000 Cluster defects <= 30 Single column Defects <=10 Dead columns = none Radiometric and geometric profile included
Filter array	Interchangeable color or color-IR
Lens	Zeiss Distagon 55.0 mm, 36° FOV
Exposure control	Automatic: aperture or shutter priority
Shutter	Electronically controlled focal plane
Shutter speed	1/125 - 1/4,000 seconds
Exposure compensation	± 2 EV in 1/3 EV steps
Exposure rate	Maximum 4 seconds**
Housing	Proprietary ruggedized and individually profiled CCD array mount. Ruggedized exoskeleton, capable of <1 pixel geometric accuracy over RTCA/DO-160D shock and vibration
Calibration	Terrestrial and airborne calibration with full report
Modular replaceability	Includes spare exoskeleton, pre-calibrated camera body and lens for instant field servicing

##### Ruggedized Data Recorder

- Integrated with ALTM control rack
- Internal pressurized 80 GB disk
- Removable 80 GB disks (2)
- Mission planning & camera trigger via ALTM-NAV
- QC thumbnail image display on ALTM-NAV

##### Image Performance

Typical at 1,500 m, 120 knots and 1/2,000 exp.

GSD: 0.25 m  
Smear: 15%

Bands	1	2	3
Color Mode, nm	400-500	500-600	600-680
CIR mode, nm	510-600	600-720	720-800

##### Physical

Size	Camera	16 x 18 x 41 cm
	Data recorder	19" rack, 3U height
Weight	Camera	5 kg
	Data recorder	10 kg
Power	Camera/data recorder	28 VDC, 4 A
	Auxiliary power unit	115 VAC
Operating temperature	0 to + 40° C	
Humidity	5 to 90% RH non-condensing	
Altitude	maximum 6,000 m	

##### Processing Software (included)

MissionVue - downloads images from removable drives

ImageVue - develops digital image

- Applies fall-off corrections and color balance
- Formats: TIFF, JPEG, IMG
- Quantization: 8 or 16 bit

POS Cal and POS EO from Applanix Corp.

ImageStation Suite from Z/I Imaging

- ISAT Aerial Triangulation Software\*\*\*

##### Option

- OrthoPro/Geomedia for orthorectification and mosaicing

Specifications subject to change without notice.

\*Specially selected from Class 1 (see Kodak KAF-16801CE.V4.pdf)

\*\*Two seconds available in a future release

\*\*\*Microstation not supplied



Images: Camera and Data Recorder



100 Wildcat Road • Toronto, ON • Canada M3J 2Z9

Tel: [416] 661-5904 • Fax: [416] 661-4168

Web: [www.optech.on.ca](http://www.optech.on.ca) • Email: [inquiries@optech.on.ca](mailto:inquiries@optech.on.ca)

© Copyright 2004, Optech Incorporated. All rights reserved. 090204



## Appendix C: Sky Research LiDAR Sensor Crater Calibration Plot

**Table C-1: Simulated Craters Dimensions**

<b>Crater ID</b>	<b>Width (m)</b>	<b>Depth (m)</b>
<b>1</b>	0.55	0.15
<b>2</b>	1.07	0.21
<b>3</b>	1.46	0.17
<b>4</b>	1.83	0.15
<b>5</b>	2.50	0.17
<b>6</b>	0.58	0.23
<b>7</b>	1.07	0.23
<b>8</b>	1.52	0.18
<b>9</b>	1.86	0.20
<b>10</b>	2.50	0.24
<b>11</b>	0.67	0.32
<b>12</b>	1.25	0.38
<b>13</b>	1.65	0.35
<b>14</b>	2.01	0.30
<b>15</b>	2.53	0.29
<b>16</b>	0.91	0.12
<b>17</b>	1.11	0.50
<b>18</b>	1.49	0.43
<b>19</b>	2.10	0.50
<b>20</b>	2.47	0.44
<b>21</b>	1.16	0.73
<b>22</b>	1.34	0.79
<b>23</b>	1.55	0.58
<b>24</b>	1.83	0.69
<b>25</b>	2.04	0.79
<b>26</b>	1.19	0.90
<b>27</b>	1.30	0.90
<b>28</b>	1.58	0.90
<b>29</b>	1.83	0.87
<b>30</b>	2.13	0.99

**Table C-2: Simulated Craters Detection Results**

<b>Crater ID</b>	<b>Crater Measurements</b>		<b>LiDAR-Derived Crater Estimates</b>	
	<b>Width (m)</b>	<b>Depth (m)</b>	<b>Width (m)</b>	<b>Depth (m)</b>
<b>1</b>	0.55	0.15	ND	ND
<b>2</b>	1.07	0.21	1.30	0.14
<b>3</b>	1.46	0.17	1.90	0.14
<b>4</b>	1.83	0.15	2.40	0.17
<b>5</b>	2.50	0.17	2.80	0.34
<b>6</b>	0.58	0.23	ND	ND
<b>7</b>	1.07	0.23	1.20	0.22
<b>8</b>	1.52	0.18	1.20	0.13
<b>9</b>	1.86	0.20	1.40	0.15
<b>10</b>	2.50	0.24	2.85	0.24
<b>11</b>	0.67	0.32	ND	ND
<b>12</b>	1.25	0.38	1.57	0.24
<b>13</b>	1.65	0.35	1.75	0.28
<b>14</b>	2.01	0.30	2.55	0.23
<b>15</b>	2.53	0.29	2.70	0.30
<b>16</b>	0.91	0.12	ND	ND
<b>17</b>	1.11	0.50	1.30	0.34
<b>18</b>	1.49	0.43	1.50	0.32
<b>19</b>	2.10	0.50	2.30	0.52
<b>20</b>	2.47	0.44	2.60	0.42
<b>21</b>	1.16	0.73	1.70	0.46
<b>22</b>	1.34	0.79	1.65	0.65
<b>23</b>	1.55	0.58	1.84	0.42
<b>24</b>	1.83	0.69	1.95	0.41
<b>25</b>	2.04	0.79	2.40	0.75
<b>26</b>	1.19	0.90	1.25	0.45
<b>27</b>	1.30	0.90	1.90	0.61
<b>28</b>	1.58	0.90	2.00	0.88
<b>29</b>	1.83	0.87	1.90	0.79
<b>30</b>	2.13	0.99	2.69	0.99